

Quantification of void shape in cemented materials

Okan Önal*, Gürkan Özden and Burak Felekoğlu

Department of Civil Engineering, Kaynaklar Yerleskesi, Buca-Izmir 35160, Turkey

(Received April 2, 2009, Accepted April 29, 2010)

Abstract. A color based segmentation procedure and a modified signature technique have been applied to the detection and analyses of complicated void shapes in cemented materials. The gray-scale segmentation and available signature methods were found to be inefficient especially for the analyses of complicated void shapes. The applicability of the developed methodology has been demonstrated on artificially prepared cemented materials made of self compacted concrete material. In order to characterize the void shapes in the investigated sample images, two new shape parameters called as coefficients of inclusion and exclusion have been proposed. When compared with the traditional use of the signature method, it was found that the methodology followed herein would better characterize complicated void shapes. The methodology followed in this study may be applied to the analysis of complicated void shapes that are often encountered in other cementitious materials such as clays and rocks.

Keywords: void shape; color segmentation; image analysis; coefficients of inclusion and exclusion.

1. Introduction

The vast majority of research on the determination of skeleton and fabric characteristics of cohesive materials with grains and voids involved study of grain characteristics. The literature is rich in research papers about size, shape, orientation and spatial distribution of grains either in sliced sections of cohesive materials or discrete aggregate samples using digital image analysis methods. Research studies on void characteristics, however, have been comparatively limited. Void distribution characteristics of soils, bituminous, concrete and rock materials were studied using digital image analysis methods in the past. Crabtree *et al.* (1984) have successfully segmented the voids in thin sections of blue dyed epoxy impregnated rock material using color segmentation technique. Masad *et al.* (1999) have studied the structural characterization of asphalt concrete using both X-ray computed tomography and conventional investigation of sliced sections via digital image processing methods. The segmentation of voids has been achieved by gray-scale segmentation technique, where a white mortar has been used to provide enough contrast while identifying air voids. Frost and Kuo (1996) have automated the Oda's methodology (1972) to determine the local void ratio of granular material in 2D sections using high level image processing techniques. Similarly, Bhatia and Soliman (1990) have determined the frequency distribution of void ratio for three granular materials having different grain characteristics using image analyzer. Obaidat *et al.* (1998) used spatial filters and image processing operations of a semi automated computer-vision system to quantify the percentage of voids in mineral aggregates of bituminous mixtures. Soroushian *et al.* (2003) have developed specimen preparation and image processing techniques focusing on concrete

* Corresponding author, Ph.D., E-mail: okan.onal@deu.edu.tr, okan.onal@gmail.com

micro cracks and voids for use in automated quantitative micro structural investigation of concrete. He utilized epoxy impregnation so that the gray-scale segmentation of the pores and cracks could be made in the scanning electron microscopy images. Ozturk and Baradan (2008) have obtained mathematical models to determine the relationship between pore structure of cement mortars and compressive strength using gray scale segmentation technique applied on the scanning electron microscope images. The above mentioned studies, however, do not cover the shape characteristics of the voids. Zhang *et al.* (2005) have investigated the roundness ratio parameters, a basic shape parameter of the air void detected using gray-scale segmentation technique. The same shape parameter for voids has been employed for foam concrete by Nambiar and Ramamurthy (2006).

This study aimed spatial distribution and shape characterization of voids in cemented materials using color segmentation and signature methods. The color segmentation has been found very beneficial while separating voids from the rest of the image. Trials for segmenting the voids in gray-scale segmentation were not proved to be efficient since either void shapes could not be captured satisfactorily or the voids and small objects in the cohesive matrix were not detected during threshold stages. The signature technique as applied in this study is similar to the form index parameter proposed by Masad *et al.* (2001). However, it has been modified in order to adapt it to the analyses of highly irregular void shapes. The signature algorithm as applied in this study enabled definition of new shape parameters that were proved to be useful in characterization of individual voids.

2. Materials

In order to demonstrate applicability of void detection and analysis algorithms, two specimens were cast using basalt coarse aggregate, river sand and ordinary Portland cement and sliced horizontally into 12 pieces. One of these specimens served as the control sample where proportioning of the mixture has been made in such a manner that minimum segregation is allowed to take place along the specimen length. The other specimen, on the other hand, has been artificially segregated by arranging mixture properties. This was made since it was noticed in authors' previous experiences that void shapes were considerably different and complicated in segregated self compacting concrete samples. Since the self-compacting concrete has the viscosity up to 10 times than that of ordinary concrete, it is possible to cast without vibration and to maintain its fluidity without segregation of material. Therefore, complicated void shapes which cause at mixing and casting of concrete remain in the concrete mixture. The image acquisition system employed throughout the study is a visual inspection unit with a USB connection to a desktop computer. Details of imaging specimens and the image acquisition system are given in the following.

2.1 Sample preparation

Two cylindrical specimens, 10 cm in diameter and 60 cm in height, were cast using ordinary Portland cement serving as the cementitious material. The well-known powder-type mix design method of self-compacting concrete (SCC) (Okamura and Ouchi 1999) has been applied to the design and production of the specimen material. In order to increase the powder amount of the mix, a C-type fly ash and limestone powder were used. Characteristics of the self-compacting mix proportions for the two specimens are given in Table 1. One should note that proportioning of self-

Table 1 SCC mix proportions

Material	Proportion	
	By weight per cubic meter, kg	By volume per cubic meter, l
Cement	360	114
Water	180	180
Inert filler (limestone)	190	74
Fly ash	140	62
Sand	740	285
Coarse aggregate	720	267
Air content	-	10
Admixture	12-36	10.9-32.7

compacting mixtures was the same except the admixture, a polycarboxylate type super plasticizer, of which proportion has been set as 3.3% and 10% of the cement weight in order to produce non-segregating and artificially segregated mixtures, respectively.

Once cast, samples were cured in lime-saturated water for 90 days. Following the curing period, samples were horizontally sliced into 12 pieces using a pit saw. According to Hilliard (1968) when a limited number of uniformly distributed test planes is cut parallel, the expected value of the area fraction of voids on test planes is an unbiased estimate of the volume fraction of voids of the specimen. In order to highlight voids on slice surfaces, sections have been plastered using jointing mortar and then sandpapered until the section surface reappeared. In this manner, voids have been filled with yellow mortar, which can be detected by means of color segmentation techniques.

2.2 Image acquisition system

Since the success of digital image processing operations greatly depends on the quality of the



Fig. 1 Visual inspection unit

captured images and the illumination conditions, a visual inspection unit housing a high precision digital camera (Canon EOS 350D), EF-S 18-55 mm Lens and three florescence light sources has been build for the acquisition of the specimen images as shown in Fig. 1. The visual inspection unit ensured constant illumination for the image acquisition. Moreover, shutter speed and aperture combination of the camera was kept the same for each captured image. Therefore, contrast, brightness and saturation parameters of the captured images varied in a narrow band, which enhanced the results of the segmentation techniques.

3. Image acquisition

The image acquisition was performed by remote shooting capability of the camera's software. The camera was controlled by the computer via USB cable connection so that a fully insulated area from the ambiance illumination was obtained during image capturing. Since both the gray-scale and color segmentation techniques were employed during image processing of an input image in the study, the aperture and shutter speed combination of the camera were set as F 5.6 - 1/13 s in order to obtain the best possible contrast and color saturation balance. The images were captured with a resolution of 3456×2304 pixels creating a field view of 182×122 mm and were directly transferred to the computer.

4. Image processing

A complete analysis of a specimen image including voids, grains and cohesive matrix requires use of both gray-scale and color segmentation. Gray-scale and color segmentation algorithms were coded using a technical computing language (Mathworks 2005) while generating the script files employed in this study. Aggregate grains were subject to gray-scale segmentation while determining the state of segregation of the SCC sample which was intentionally cast with a soft cohesive matrix. The images have been transformed from RGB format into gray scale, in order to apply gray scale segmentation technique. A proper threshold value has been calculated using Otsu (1979) methodology. The gray scale images have been converted into binary images where the two levels are assigned to pixels that are below or above the specified threshold value. The color based segmentation, however, was utilized for the detection of voids within the specimens. The extracted features of the images such as grains and voids were investigated by the image analysis functions of an image processing toolbox for the determination of the spatial distribution and shape characteristics. On the other hand, it was necessary to develop a specific script code for the extraction of the digital signatures of the voids and analysis of irregular void shapes.

4.1 Color segmentation

Color segmentation has been performed using L*a*b* color space (a coordinate system and a subspace within that system where each color is represented by a single point) for the determination of voids in 2D sections. The L*a*b* color space model (Robertson 1997) has been introduced as a device independent color model enabling quantification of visual differences in any digitized image since influence of illumination conditions could be easily normalized in this space by tracing any

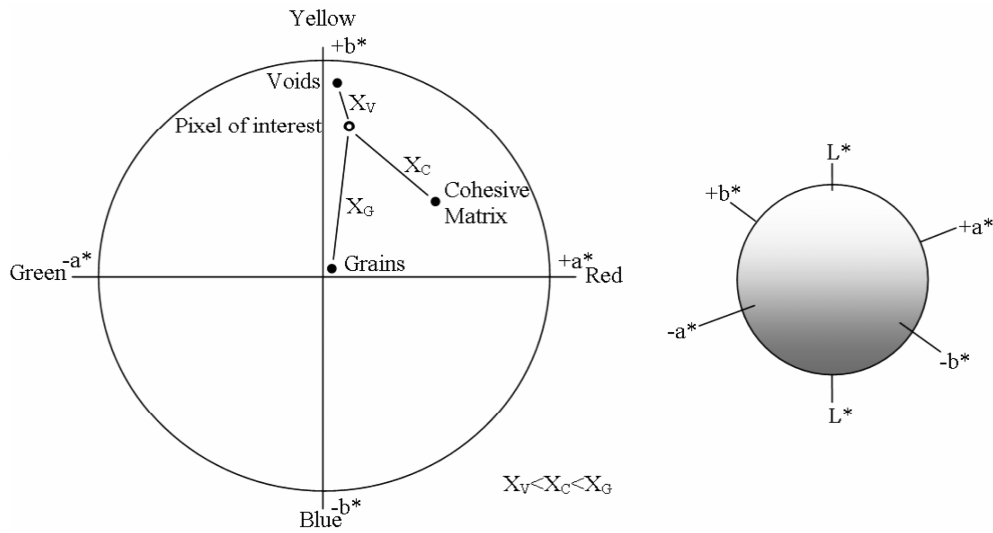


Fig. 2 $L^*a^*b^*$ color space model in color segmentation

deviations in lighting conditions in L^* layer. The $L^*a^*b^*$ color space consists of the luminosity ' L^* ' or brightness layer, the chromaticity layer ' a^* ' indicating the location of the color along the red-green axis, and the chromaticity layer ' b^* ' indicating the location where the color falls along the blue-yellow axis (Fig. 2). During color segmentation, therefore, captured images were transformed into $L^*a^*b^*$ space firstly.

It has been necessary to define only specific colors in the original image so that color segmentation could be performed satisfactorily without increasing computational effort and complexity of the algorithm. Four specific colors were selected in the slices of the specimens for this purpose. The selection has been made visually depending on the appearance of the original image. Two tones of yellow colors were selected for the voids, in order to avoid erroneous segmentation, since color transition from the voids to the cohesive matrix in captured images takes place gradually. The grain objects and the cohesive matrix, on the other hand, were related to the black and gray color, respectively. The average a^*b^* values for each color were calculated in the $L^*a^*b^*$ color space for each selected color. Color classification is made based on the closest Euclidian distance of each pixel to these average values in color space (Fig. 2). The classified pixels have been stored as different layers in a matrix. Following color segmentation, two tones of the yellow layers that were detected in the images have been merged together and transformed to binary form while generating the final image. The flow chart diagram of the color segmentation process for void detection is given in Fig. 3.

5. Image analysis

The image segmentation (i.e. segmented voids in Fig. 3(e)) is followed by the characterization of the regions. A region map, where labels are assigned to pixels has been generated using the eight adjacency pixel relationship. In this manner, a new matrix carrying label information is formed so that quantitative information about the objects could be obtained examining their properties in this

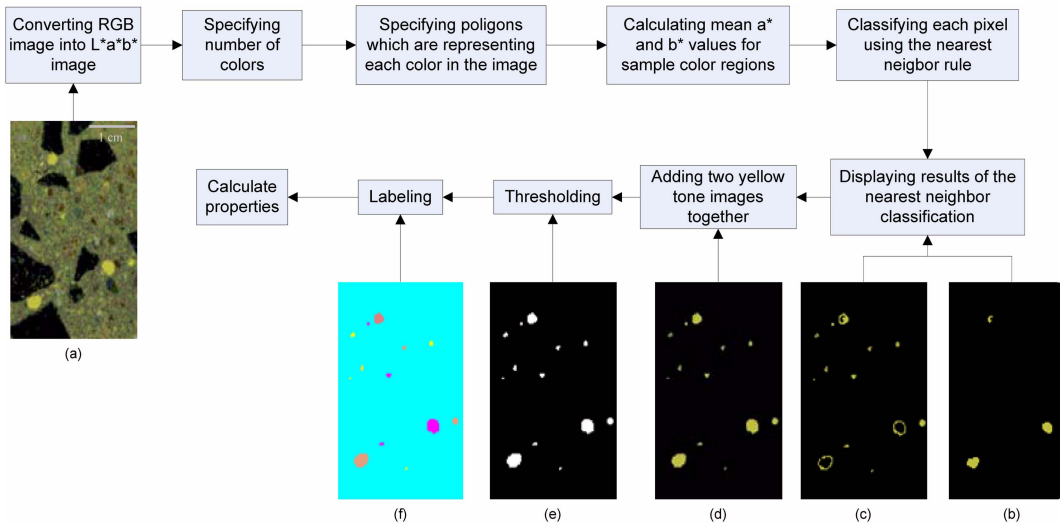


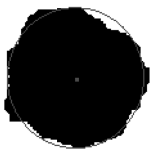



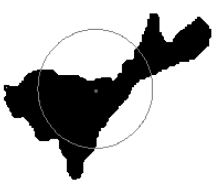
Fig. 3 Image processing flow chart of void detection by color segmentation

matrix. For instance the area, centroid and circumference of the objects in the region map have been extracted using the Matlab image processing toolbox functions that enable calculation of the area ratio and spatial distribution of the grains and voids. Moreover, the characteristics of the voids have been numerically expressed using the roundness parameter, R , which is defined as $R = (4 \cdot \pi \cdot \text{area}) / (\text{perimeter})^2$ where area and perimeter are given in pixels for each void and the eccentricity parameter, which is defined with respect to the axes of an ellipse whose second moment is equal to that of the shape using the below equation

$$e = \sqrt{1 - \frac{b^2}{a^2}} \quad (1)$$

One can notice in the above given equation that the ellipse parameter varies between 0 and 1.

Table 2 Shape characteristics of typical void images

Shape					
Roundness ratio (R_r)	0.81	0.76	0.18	0.33	0.26
Eccentricity(e)	0.35	0.63	0.64	0.82	0.92
Coefficient of inclusion (c_i)	0.046	0.107	0.327	0.184	0.392
Coefficient of exclusion (c_e)	0.045	0.087	0.243	0.366	0.590
$c_e - c_i$	-0.001	-0.020	-0.084	0.182	0.189
$c_e + c_i$	0.091	0.107	0.570	0.550	0.982

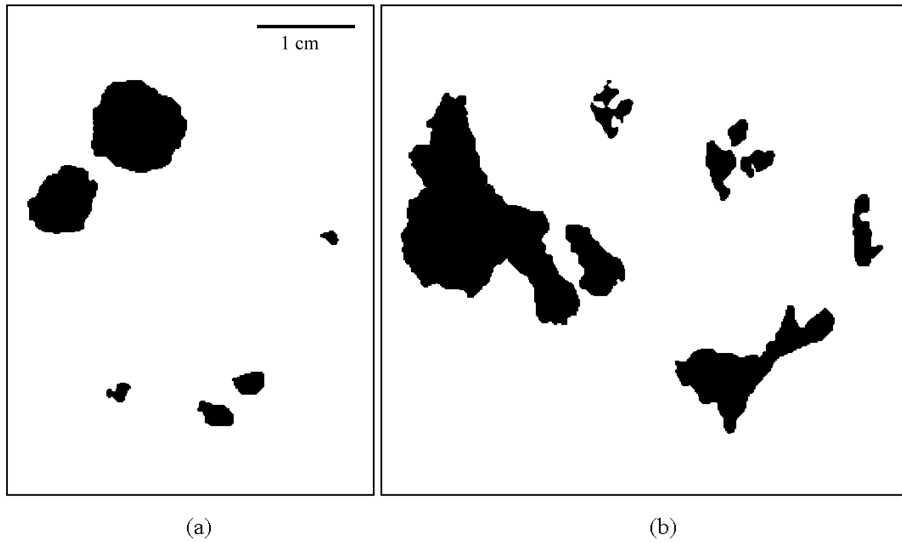


Fig. 4 Void shapes in (a) non-segregated and (b) segregated specimens

Values of 0 and 1 define two degenerate cases; an ellipse whose eccentricity is 0 being a circle and an ellipse whose eccentricity is 1 being a line.

The eccentricity values of the void shapes in non-segregated and segregated samples are given in Table 2. The eccentricities for the void shapes in the segregated sample converge to unity, where the same parameters for the circular voids decrease depending on the degree of elongation. The roundness parameter has been computed for void shapes in the segregated and non-segregated sample images. A sample image for the illustration of voids in segregated and non-segregated is shown in Fig. 4 where some portion of the voids in a slice is given. It can be noticed in Table 2 that the roundness ratio converges to unity for a perfectly circular void and diverges from unity depending on the distortion of the void shape. The same parameter has been used for void analyses by Lange *et al.* (1994) and Zhang *et al.* (2005).

In the segregated sample, the void shapes are more irregular when compared with those in the non-segregated one, and the roundness ratio parameter is not sufficient to completely characterize a void shape alone as one can notice in Table 2. The same is also valid for the eccentricity parameter. In order to provide supplementary tools, additional parameters such as the coefficient of inclusion, c_i , and the coefficient of exclusion, c_e , can be defined.

The coefficients of inclusion and exclusion are defined by evaluating the signature of the void shape with respect to an equivalent circle of which area is equal to that of the void. The circle is positioned at the centroid of the void being analyzed (Fig. 5(a)). The evaluation process starts by assigning a specific value to each border pixel. This is performed by taking the difference between the Euclidean distance of a pixel, d_p , which is defined as the distance from the border of the void shape to the center of the equivalent circle and the radius of the equivalent circle, r_e . This value is later normalized with respect to the radius of the equivalent circle yielding the ordinate of the signature of the void as given in Eq. (2) and shown in Fig. 5(b). The abscissa of this figure is set as the number of pixels along the void shape border as explained in the following.

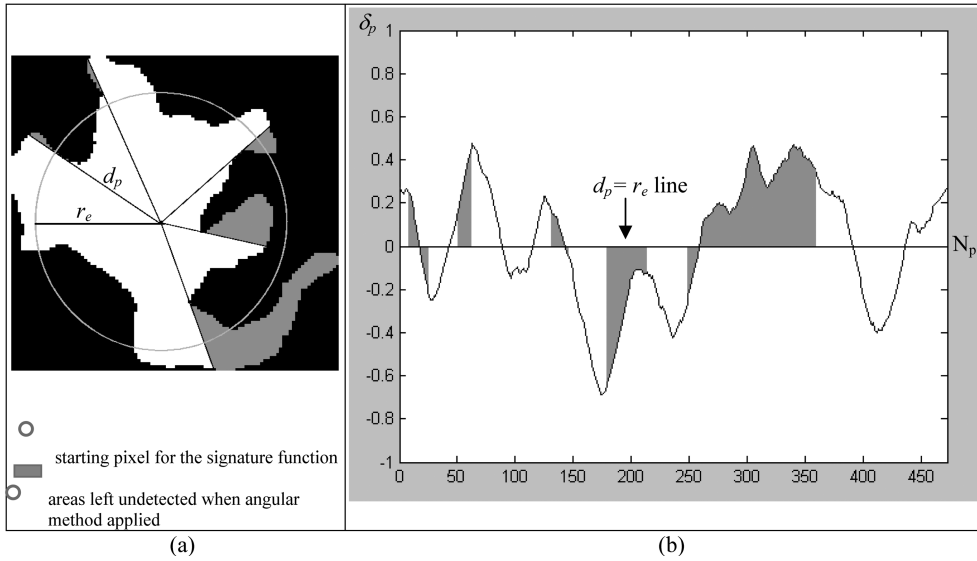


Fig. 5 (a) The equivalent circle, (b) digital signature of the void shape using the perimeter method

$$\delta_p = \frac{d_p - r_e}{r_e} \quad (2)$$

The coefficient of exclusion is described as the ratio of the sum of the positive values of δ_p to the number of positive valued ordinates of the signature. Namely, this procedure gives the average of the positive side of the signature. The same is also valid for the negative side resulting in the calculation of the coefficient of inclusion. The methodology followed here to obtain the signature of the void shape differs from its predecessors (Masad *et al.* 2001) by using the number of pixels, N_p , along the perimeter as the abscissa of the signature function instead of angle increments during scanning of the shape. Such a methodology has been found necessary for complete evaluation of the irregularly shaped voids since the angular increment method has failed to detect complicated border shapes. This fact can be better demonstrated by comparing the coefficients of exclusion and inclusion that were computed using both methods. The angular scanning method yielded 0.203 and 0.249 for exclusion and inclusion coefficients, respectively. The perimeter method, on the other hand, resulted in 0.251 and 0.240 for the same parameters. The difference between these methods is due to the presence of shaded areas left untouched during the angular scanning procedure as illustrated in Figs. 5(a) and 5(b).

6. Results and discussions

Since one of the artificially prepared samples was intentionally segregated by means of additives, image analysis algorithms were expected to capture non-uniform grain and void distribution along sample length. This aspect of the study is shown in Fig. 6 where digital images of the upper faces of the slices along sample length are given. Non-uniform grain and void distributions of the segregated sample are visible in Figs. 6(b) and 6(d), respectively. Please note that the fourth section

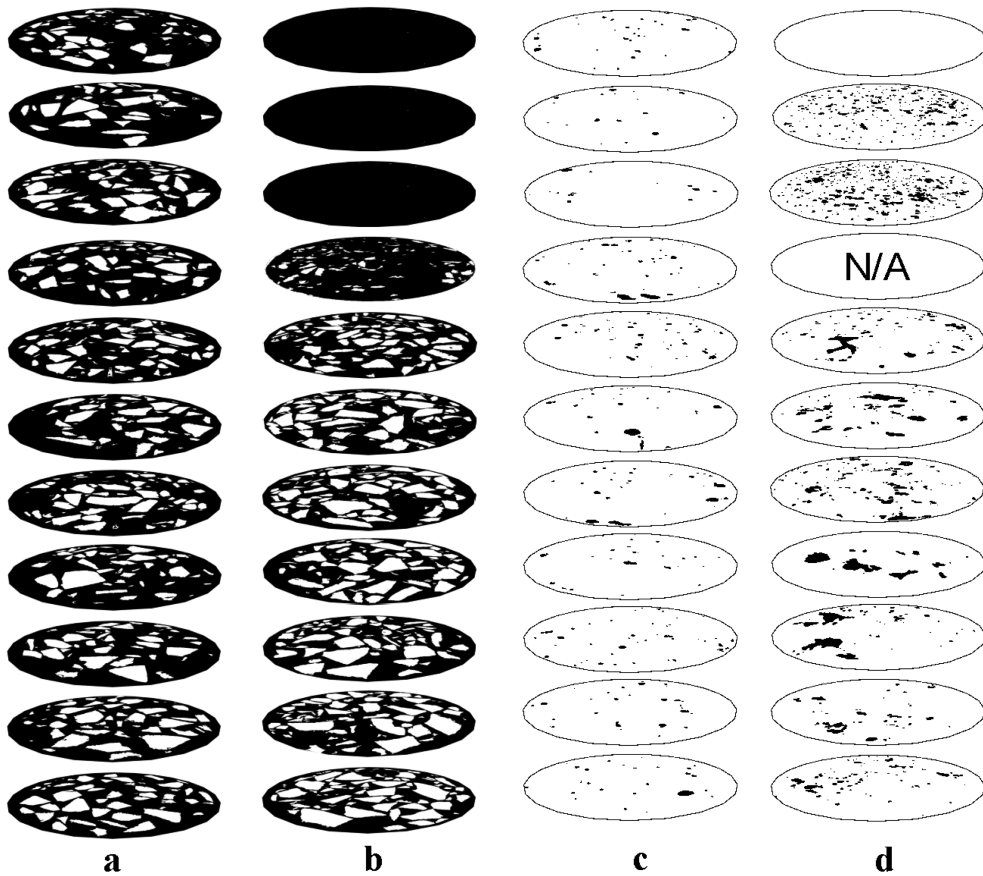


Fig. 6 (a) Grain distribution for the non-segregated specimen, (b) grain distribution for the segregated specimen, (c) void distribution for the non-segregated specimen, (d) void distribution for the segregated specimen

from the top have not been captured, since the excessive segregation of the concrete. The other sample, on the other hand, exhibits quite uniform distribution since the cohesive matrix of this sample was able to provide enough resistance to avoid segregation (Figs. 6(a) and 6(c)). Porosity values for each specimen section have been computed using the binary images resulted from the color segmentation process. The variation of the ratio of the total void area in a section to the total area of this section along the specimen length has been presented as porosity values in Fig. 7 where random distribution of the porosity parameter in the segregated sample is remarkable.

The cohesive matrix characteristics have an influence on the void shape as noted in the previous sections. A closer look to the slice images revealed that voids of the segregated sample are more rounded compared with those of the segregated sample. The shape characteristics that are defined in the previous section for void images can effectively describe attributes of a void when they are used in combination. For instance, it can be noticed that the roundness parameter in Table 2 may be sufficient while defining a round or nearly round void shape. However, it is not possible to handle complicated void shapes using either the roundness or the eccentricity parameter alone. The eccentricity parameter is a common way of definition of the elongation characteristic of any shape in image processing. It is notable in Table 2 that the orientation of the second void shape from left

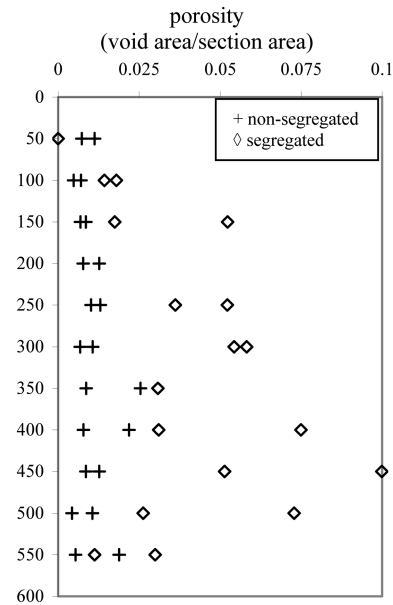


Fig. 7 Porosity variation along specimen length

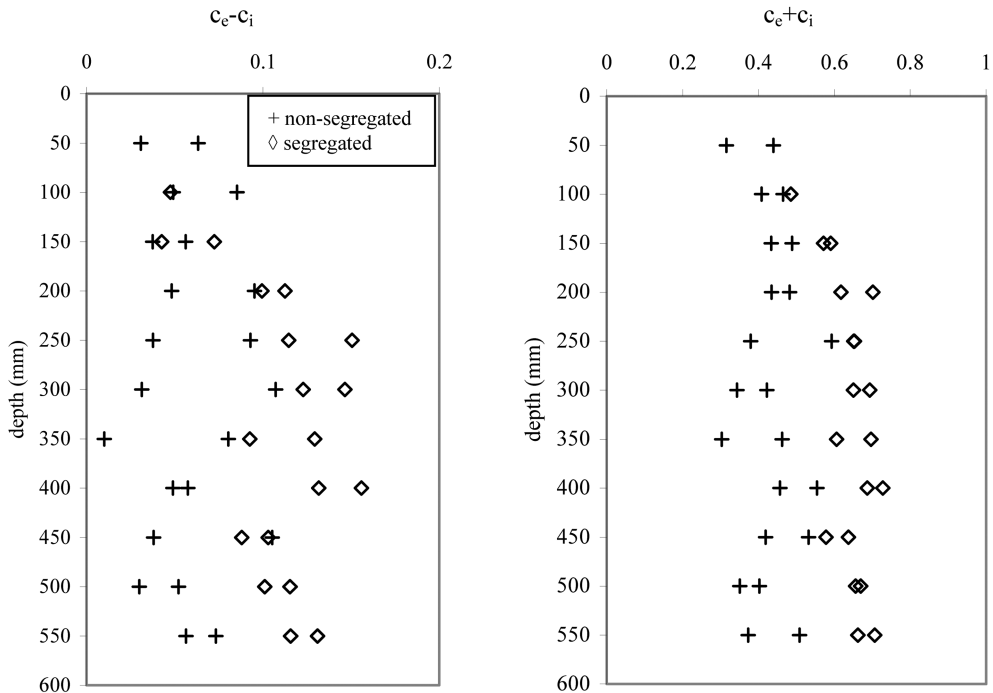


Fig. 8 (a) The difference and (b) the sum of the coefficients of exclusion and inclusion

can be captured by the help of the eccentricity parameter, which is considerably larger than that of its left neighbor. On the other hand, the roundness and eccentricity parameters do not yield enough information about the third and following voids from the left in Table 2. The third image, for

instance, has the highest perimeter length with respect to its area and there are gaps inclusive with respect to the overall shape of the void. This shape can be quite effectively defined by the help of the coefficient of inclusion, the coefficient of exclusion and the difference of these two parameters. The high inclusion coefficient means that the length of the perimeter remained inside the equivalent circle is a large value. The difference between the coefficient of exclusion and the coefficient of inclusion tells that the shape is an inclusive one with large gaps inside the equivalent circle. The low value of the roundness ratio parameter cannot describe the inclusive feature of this shape since its absolute value describes a highly elongated shape which is not the case. It is not possible to acquire an idea about the actual shape of this void during an automated image analysis operation by only using the roundness ratio and the eccentricity parameters.

The sum of inclusion and exclusion parameters ($c_e + c_i$) is a measure for the severity of a distorted image with respect to an ideal circle. The value of ($c_e - c_i$) better describes the actual shape of a void since its negative and positive values tell that the void has either an inclusive or an exclusive shape. A $c_e - c_i$ value very close to zero means that the shape is nearly a circle (the first void in Table 2). A highly negative value tells that the shape has large gaps inside the equivalent circle (the third void). A highly positive value, on the other hand, corresponds to an elongated shape void. A second level differentiation the fourth and fifth voids can be made by considering the value of ($c_e + c_i$).

The mean values of the difference and sum of the coefficients of inclusion and exclusion have been calculated for each slice image as presented in Fig. 8. The void shapes, appearing more elongated in the segregated sample, are classified as exclusive shapes. The values of the $c_e - c_i$ parameter in the slices of the segregated sample are higher when compared with the non-segregated one (Fig. 8(a)). The intensity of the distortion of the voids in the segregated sample is shown in Fig. 8(b). One can notice in both figures that the coefficient of inclusion and exclusion can effectively characterize void shapes in the investigated samples.

7. Conclusions

It has been noticed that color segmentation can be effectively used if several different objects with varying colors exist in the original image. The color segmentation process as employed in this study generated several object layers for each color group in the image, which enabled individual analyses of the desired object group in the image. In order to characterize the void shapes in the investigated sample images, two new shape parameters called as coefficients of inclusion and exclusion have been developed. In addition to the well known roundness ratio and eccentricity shape parameters, these two parameters along with their sum and difference values have been used in the characterization of the highly irregular void shapes. The developed parameters may also have potential use as supplementary features in the neural network applications or object recognition processes in the digital image analysis applications. The methodology followed in this study may be applied to the analysis of complicated void shapes that are often encountered in other cementitious materials such as clays and rocks.

References

Bhatia, S.K. and Soliman, A.F. (1990), "Frequency distribution of void ratio of granular materials determined by

- an image analyzer”, *Soils Found.*, **30**(1), 1-16.
- Crabtree, S.J., Ehrlich, Jr. R. and Prince, C. (1984), “Evaluation of strategies for segmentations of reservoir rocks”, *Comput. Vis. Graphics Image Proc.*, **28**(1), 1-18.
- Frost, J.D. and Kuo, C.Y. (1996), “Automated determination of the distribution of local void ratio from digital images”, *Geotech. Test. J.*, **19**(2) 107-117.
- Hilliard, J.E. (1968), *Measurement of volume in volume, quantitative microscopy*, R.T. DeHoff and F.N. Rhines, eds, McGraw-Hill, New York.
- Lange, D.A., Jennings, H.M. and Shah S.P. (1994), “Image analysis techniques for characterization of pore structure of cement-based materials”, *Cement Concrete Res.*, **24**(5), 841-853.
- Masad, E., Muhunthan, B., Shashisbar, N. and Harman, T. (1999), “Internal structure characterization of asphalt concrete using image analysis”, *J. Comput. Civil Eng.*, **13**(2), 88-95.
- Masad, E., Olcott, D., White, T. and Tashman, L. (2001), “Correlation of fine aggregate imaging shape indices with asphalt mixture performance”, *Transport. Res. Record*, **1757**, 148-156.
- Mathworks (2005), MATLAB technical computing language version 7 and image analysis toolbox version 4.2, Natick, MA.
- Nambiar, E.K.K. and Ramamurthy, K. (2007), “Air-void characterization of foam concrete”, *Cement Concrete Res.*, **37**, 221-230.
- Obaidat, M.T., Al-Masaeid, H.R., Gharaybeh, F. and Khedaywi, T.S. (1998), “An innovative digital image analysis approach to quantify the percentage of voids in mineral aggregates of bituminous mixtures”, *Can. J. Civil Eng.*, **25**(6), 1041-1049.
- Oda, M. (1972), “Initial fabrics and their relations to mechanical properties of granular materials”, *Soils Found.*, **12**(1), 17-36.
- Okamura, H. and Ouchi, M. (1999), “Self-compacting concrete, development, present use and future”, *Proceedings of the First International RILEM Symposium on Self-Compacting Concrete*, Ed.: Rilem Publications s.a.r.l., Stockholm, 3-14.
- Otsu, N. (1979), “A threshold selection method from gray-level histograms”, *IEEE T. Syst. Man Cy.*, **9**(1), 62-66.
- Ozturk, A.U. and Baradan, B. (2008), “A comparison study of porosity and compressive strength mathematical models with image analysis”, *Comput. Mater. Sci.*, **43**(4), 974-979.
- Robertson, A.R. (1997), “The CIE 1976 color difference formulae”, *Color Res. Appl.*, **2**, 7-11.
- Soroushian, P., Elzafraney, M. and Nossoni, A. (2003), “Specimen preparation and image processing and analysis techniques for automated quantification of concrete micro cracks and voids”, *Cement Concrete Res.*, **33**(12), 1949-1962.
- Zhang Z., Ansari, F. and Vitillo, N. (2005), “Automated determination of entrained air-void parameters in hardened concrete”, *ACI Mater. J.*, **102**(1), 42-48.